Available online at www.sciencedirect.com
ScienceDirect
Geoderma 139 (2007) 38–50
GEODERMA
www.elsevier.com/locate/geoderma

Fibrous-clay mineral formation and soil evolution in Aridisols of northeastern Patagonia, Argentina

P.J. Bouza [a,*], M. Simón [b], J. Aguilar [c], H. del Valle [a], M. Rostagno [a]

[a] Centro Nacional Patagónico, CONICET, Avd. Brown s/n, 9120, Puerto Madryn, Chubut, Argentina
[b] Departamento de Edafología, EPS — CITE II B, Cañada San Urbano, Universidad de Almería, 04120 Almería, Spain
[c] Departamento de Edafología y Química Agrícola, Facultad de Ciencias, Universidad de Granada, C/Fuente Nueva s/n, 18002, Granada, Spain

Received 22 December 2005; received in revised form 14 December 2006; accepted 3 January 2007
Available online 26 February 2007

Abstract

Recent studies of soil–landscape relationships in northeastern Patagonia identified fibrous-clay minerals in calcic and petrocalcic horizons developed on old fluvio-glacial plains called "Rodados Patagónicos" (RP). The objectives of this study were: i) to evaluate the occurrence of fibrous-clay minerals in the arid soil environment, and ii) to establish the relationship between the soil properties and degree of the calcic horizon development, including the age of the soils containing fibrous-clay minerals in extra-Andean Patagonia. The soil studied were Calciargids, Natrigypsids, and Petrocalcids, located at elevations of 50, 70, and 130 m a.s.l., respectively. The soils are polygenetic, where the clay mineralogy is related to the age of the pedogenetic periods that affected the formation of geomorphic surfaces. In the surface horizons, illite proved to be the dominant clay mineral and was slightly altered to interstratified illite–smectite and smectite. An older pedogenic episode was identified in argillic and calcic horizons, in which smectite was prevalent. The following soil-formation period was recorded in calcic and calcic-gypsic horizons appearing in the upper limit of the RP. In these horizons, palygorskite is the dominant clay mineral. Pedogenetic carbonate was qualified as low-Mg calcite, indicating that during its precipitation, the Mg^{2+} activity increased in the soil solution, favoring the smectite→palygorskite transformation. The soil environment, favorable for this transformation, was the textural transition between the fine materials of sub-surface horizons and the coarsest deposit of RP, where temporary waterlogging occurred. The petrocalcic horizons, and their re-transported fragments, represent the oldest pedogenetic period, where sepiolite was the dominant clay mineral. During the calcretization processes, the sepiolite was precipitated from the soil solution following the formation of palygorskite. Fluorite was identified in the petrocalcic horizon, and its association with calcite and sepiolite indicated a successive precipitation of these minerals under alkaline conditions during evaporation processes.
© 2007 Elsevier B.V. All rights reserved.

Keywords: Palygorskite; Sepiolite; Fluorite; Soil genesis; Calcic and petrocalcic horizons; Chubut province of Argentina

1. Introduction

Palygorskite and sepiolite are clay minerals of fibrous morphology that are present in several environments, such as marine and lake sediments, in arid soils, and in places near hydrothermal activity. For pedogenetic and sedimentary environments, at least three hypotheses have been proposed to explain the presence of palygorskite and sepiolite: 1) inheritance from parent materials (Paquet and Millot, 1973; Khademi and Mermut, 1998, 1999), 2) detrital origin either by aeolic additions (Coudé-Gaussen, 1987) or by transport of alluvial materials (Khademi and Mermut, 1998), and 3) autigenesis in soils of arid regions (Elprince et al., 1979). According to this last hypothesis, palygorskite can be formed in flood plains and alluvial fan soils affected by fluctuations of the water table (Abtahi, 1977; Pimentel, 2002), by alteration or transformation of Mg-rich smectite (Yaalon and Wieder, 1976), or by neoformation from the soil solution (Singer and Norrish, 1974; Monger and Daugherty, 1991).

The formation of sepiolite is relatively rare in soils due to its instability in the soil environment (Zelazny and Calhoun, 1977; Singer, 1989; Singer et al., 1995). Nevertheless, sepiolite was associated to mature calcretes of pedogenetic origin and their formation is related to calcite precipitation processes (Hay and

* Corresponding author. Tel.: +54 2965 45 1024; fax: +54 2965 45 1543.
E-mail address: bouza@cenpat.edu.ar (P.J. Bouza).

0016-7061/$ - see front matter © 2007 Elsevier B.V. All rights reserved.
doi:10.1016/j.geoderma.2007.01.001

Wiggins, 1980; Watts, 1980; Singer et al., 1995; Brock and Buck, 2005).

The formation and stability conditions of fibrous-clay minerals require an alkaline environment and relatively high activities of $H_4SiO_4^0$ and Mg^{2+} (Velde, 1985; Jones and Galán, 1988; Singer, 1989). The palygorskite also requires an adequate input of Al (Singer, 1989). High ionic activities are reached only at sites with poor drainage, and therefore these fibrous-clay minerals form in confined environments. The stability of palygorskite can be explained based on three variables: pH, pMg, and pH_4SiO_4 (Singer and Norrish, 1974). At a slightly acid pH (<5.9), palygorskite would be stable at very high $H_4SiO_4^0$ and Mg^{2+} concentrations (pH_4SiO_4=2.6 and pMg=2.0), which are very rare in soils. On the other hand, at alkaline pH values (≈9.0) the stability of the palygorskite can be maintained at low Mg^{2+} concentrations (pMg>7) and at high $H_4SiO_4^0$ concentrations, or at low $H_4SiO_4^0$ concentrations (pH_4SiO_4>4) and at high Mg^{2+} concentrations. Sepiolite requires similar soil solution conditions for its formation. Consequently, the stability of these fibrous minerals is limited to arid and semiarid regions.

In areas with more than 300 mm of average annual rainfall, palygorskite is weathered into smectite (Paquet and Millot, 1973). Sepiolite is even less stable than palygorskite and can be weathered into smectite by climatic shift (Singer et al., 1995). Therefore, both fibrous-clay minerals are climatically sensitive, and can be used for the analyses of paleosols and old sedimentary sequences (Wright and Tucker, 1991).

In arid regions, the pedogenic formation of palygorskite and sepiolite is closely associated with the calcic horizon and calcrete development. Watts (1980) indicated that the pedogenesis of palygorskite and sepiolite might be related to the release of Mg^{2+} by high-Mg to low-Mg calcite transformation at high pH values. In relation to the increase in the pedogenic carbonate content, Bachman and Machette (1977), studying Aridisols of the southwestern United States, found the following sequence: illite–smectite → smectite → palygorskite → sepiolite, which is highly time-dependent (Birkeland, 1984).

In Argentina, few studies examine the presence of fibrous-clay minerals in soils. Morrás et al. (1981, 1982) suggested the presence of fibrous clays in halomorphic soils of Santa Fe Province (northeastern Argentina) affected by fluctuations in the water table. In the northeast of central Patagonia, Vogt and Larqué (1998) found small amounts of sepiolite in old gravelly alluvial deposits ("Rodados Patagónicos") of Plio-Pleistocene age affected by permafrost conditions, which can be compared to very confined environments.

Studying soil–landscape relationships on "Rodados Patagónicos" plains on the Península Valdés, Bouza et al. (2005) described the palygorskite occurrence associated with calcic horizons, assigning them a Middle-Late Pleistocene age. These authors proposed that the palygorskite was formed from the transformation of pre-existing smectites.

The objectives of the present study were: i) to evaluate the occurrence of fibrous-clay minerals in an arid soil environment, and ii) to establish the relationship between the soil properties and degree of the calcic horizon development, including the age of the soils containing fibrous-clay minerals in extra-Andean Patagonia.

2. Materials and methods

2.1. Study area

The study area is located in the northeast of Chubut province, Argentina (Fig. 1). Its geology is represented mainly by siliceous volcanic rocks of the Marifil Formation (Upper Triassic–Middle Jurassic), by the marine sedimentites of Puerto Madryn Formation (Middle Miocene) and by the sandy-gravel deposits called "Rodados Patagónicos" (RP) of Plio-Pleistocene age (Haller, 1981; Haller et al., 2001). The Quaternary, which partially covers these geological units, is formed by colluvial, alluvial, aeolic, and coastal marine deposits. Puerto Madryn Formation is composed of psamites, and pelites with some interleaves of gypsum layers. Its outcroppings are found primarily in coastal cliffs and in the erosion fronts of the great endorreic basins (salines).

The marine Tertiary is buried by the RP deposits, forming wide plains with a plateau shape. The genesis of this geological unit is related to old glaciofluvial and pluviofluvial plains widely distributed in this area and generated during the Cenozoic glaciations and deposited in an arid periglacial environment (Mercer, 1976). This plain is composed of several levels of terraces descending from the SW to NE, with altitudes varying from 750 m a.s.l. in the southeast of Chubut province to 90 m a.s.l. near the city of Puerto Madryn. In the Península Valdés area, the RP forms a relict surface 70 m a.s.l., while the most extensive plains are 50 m a.s.l. The RP deposits are comprised of sandy-gravel sediments mainly of acidic volcanic composition.

During Pleistocene glaciations the above-mentioned deposits were affected by cryogenic processes, which are registered by fossil ice-wedge casts, mainly in the highest levels of terraces, and a three-dimensional reticulate structure resembling columns and windows. The ice-wedge casts and columns are moderately consolidated by the allochthonous filling of fine sediments, carbonates, and occasionally gypsum of aeolic origin (Vogt and del Valle, 1994). The upper part of RP deposits is associated with a calcretization zone of varied morphology (del Valle and Beltramone, 1987). The plains of RP in the study area are discontinuously covered by aeolic deposits assigned to the late Glacial/Holocene period (Trombotto, 1998).

In the present work, soil profiles that developed on the three levels (50, 70 and 130 m a.s.l.) of the RP plateaus were studied: two in the Península Valdés (PV1 on the surface at 50 m a.s.l., and PV2 on the surface at 70 m a.s.l.), and a third soil on the ranch called "El Ranchito" (ER, in the surface at 130 m a.s.l.), located 90 km west of Puerto Madryn city (Fig. 1). Fig. 2 shows an aspect of the RP outcrops.

In the Península Valdés the average annual rainfall is 246 mm and the average temperature is 12.5 °C. The PV1 and PV2 vegetation consist of a shrubby herbaceous steppe with *Chuquiraga avellanedae* and *Stipa tenuis* being the most prevalent species. The average annual rainfall at the ER site is 170 mm and the average annual temperature is 13.5 °C. The

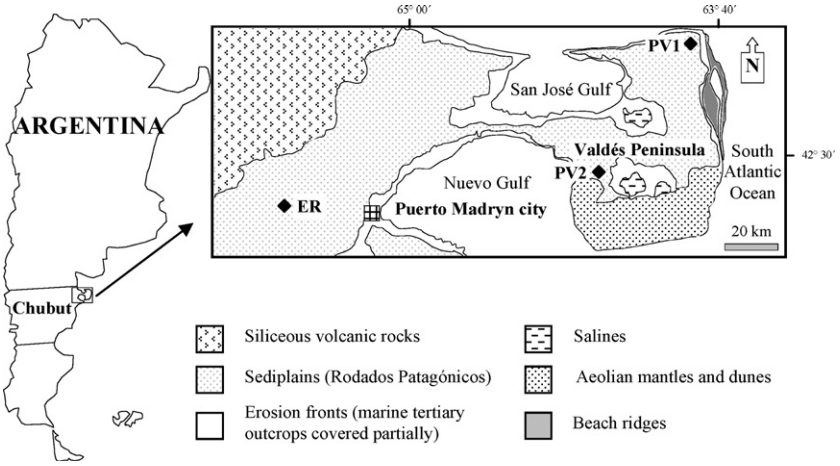

Fig. 1. Location and some geomorphological features of the region and situation of the region studied.

vegetation consists of a shrubby steppe of *Larrea divaricata* with scattered individuals of *S. tenuis*.

A common attribute, as in most Patagonian Aridisols, is the polygenetic feature characterized by successive geomorphic episodes alternating with pedogenic episodes having wetter climatic conditions than at present (Bouza et al., 2005).

2.2. Morphological and analytical determinations

The morphological description and classification of the soils were according to the Soil Survey Staff (1999). Each soil sample was air-dried and screened (2 mm mesh size) to separate the gravel and estimate its percentage. In the fine earth, the particle-size distribution was determined by the pipette method after removal of organic matter with H_2O_2 30% and carbonate with Na-acetate buffer solution at pH 5.0 (Gee and Bauder, 1986). The $CaCO_3$ equivalent was determined by a manometric method (Williams, 1948) and the gypsum content by the electroconductometric method (U.S. Salinity Laboratory Staff, 1954). The organic carbon content (OC) was determined using the method of Tyurin (1951). The cation-exchange capacity (CEC) was determined by saturating samples with 1 N Na-acetate at pH 8.2. The exchangeable Na^+ was extracted with 1 N NH_4^+-acetate at pH 7.0 and measured by flame photometry. Total chemical analysis (expressed as percentage of oxides) was determined on the fine earth (<2 mm) by X-ray fluorescence using a Philips PW-1404 instrument. The molar ratios (percentage of oxide divided by molecular weight) Mg:Al and Si:Al were calculated.

A saturation extract (SE) was prepared from the fine earth and, after 24 h, the solution was vacuum pumped, and its pH and electrical conductivity (EC) were measured. The Ca^{2+} and Mg^{2+} contents in the SE were determined by atomic-absorption spectroscopy, the Na^+ and K^+ by flame photometry, and the Cl^-, F^- and SO_4^{2-} by ion chromatography (Dionex 120). The carbonate alkalinity was determined by acid titration with 0.01 N H_2SO_4. From these results, the exchangeable-sodium percentage (ESP) was estimated (U.S. Salinity Laboratory Staff, 1954). Soluble silica was quantified by the blue silicomolybdous acid procedure (Hallmark et al., 1982). The ionic strengths (I) were determined by $I=1/2\Sigma ciZi^2$, where ci is the concentration in moles liter^{-1} of ion i and Zi is the valency of that ion. Activity coefficients were derived by the Davies' equation (Lindsay, 1979).

The mineralogy of the soils was estimated from powder bulk samples and oriented clay fraction without carbonates by XRD techniques using a Philips PW-1700 instrument with CuKα radiation. The samples of clay fraction were prepared according to two treatments: 1) Mg-saturated, air-dried; and 2) Mg-saturated ethylene glycol solvated. The diffraction intensities used in the semi-quantitative analysis were taken from Schultz (1964) and Barahona (1974). The micro-morphological study was based on thin-section descriptions (Bullock et al., 1985). On the same clay samples used to XRD analysis, a Zeiss-950 scanning electron microscope (SEM) was used to examine the morphology of clay particles. Alternatively, a Jeol JSM 6460 LV scanning electron microscope with a EDAX PW 7757/78 X-ray energy-scattering micro-analyzer (SEM-EDS) was used to determine the composition of certain clay particles.

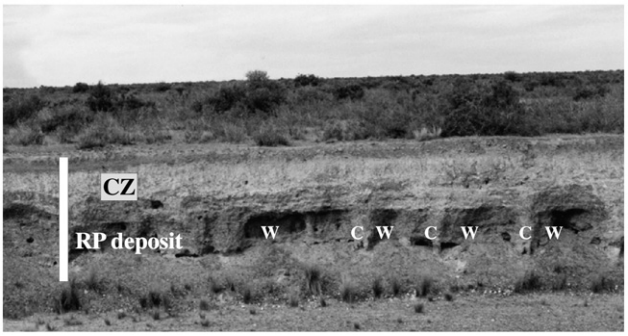

Fig. 2. The outcrop of the "Rodados Patagónicos" in "Península Valdés". Calcrete zone (CZ); cryogenic morphologies: columns (C) and windows (W), bar scale=2 m.

3. Results

3.1. Soil characteristics

As mentioned above, the RP appear deep in the three geomorphic surfaces, but the soils clearly differed in their morphological, physical, and chemical characteristics (Fig. 3;

Tables 1 and 2). The morphologic soil descriptions showed lithologic discontinuities, which delimit successive depositional units, these being alternatively affected by pedogenetic processes.

Site PV1 represents the youngest geomorphic surface. The soil had a deep carbonate accumulation (26%) that affected the upper part of the RP, constituting the 3Ck2 horizon. This surface was presumably eroded and later covered by a deposit in which carbonate leaching, weathering, and clay illuviation would have taken place, forming the sequence of 2Bt-2Btk-2Ck1 horizons. The fraction >2 mm contained rounded fragments of petrocalcic crusts, which increased in the 2Ck1 horizon (0.6% in the 2Btk horizon and 9.9% in the 2Ck1 horizon). The fragments of greater size reach 10 cm maximum diameter in the transition with the 3Ck2 horizon (Fig. 3). The 2Bt horizon had a sandy–clay–loam texture and a moderate, medium, sub-angular blocky structure.

Clay illuviation was evident in thin sections by the presence of clay coatings (<30 μm) on mineral grains and on void walls. The carbonate material in the soil matrix of the 2Btk horizon was generally powdery, with diffuse patches and hardened nodular accumulations, whereas in the 2Ck1 horizon the carbonates constitute layers of massive structure. The micromass of these calcic horizons was composed mainly of micrite to micro-sparite size, clay particles, unidentified mafics, iron oxides, and opaques. The b-fabric was crystallitic, and, in very restricted areas, it was striated and stipple-speckled. A common feature was the presence of matrix nodules, floating coarse mineral components (Fig. 4a–b) and micritic calcite nodules surrounded by circum-granular cracks (Fig. 4b–c). Subsequent calcite crystallizations were frequently observed on the edges of petrocalcic crust fragments (Fig. 4c).

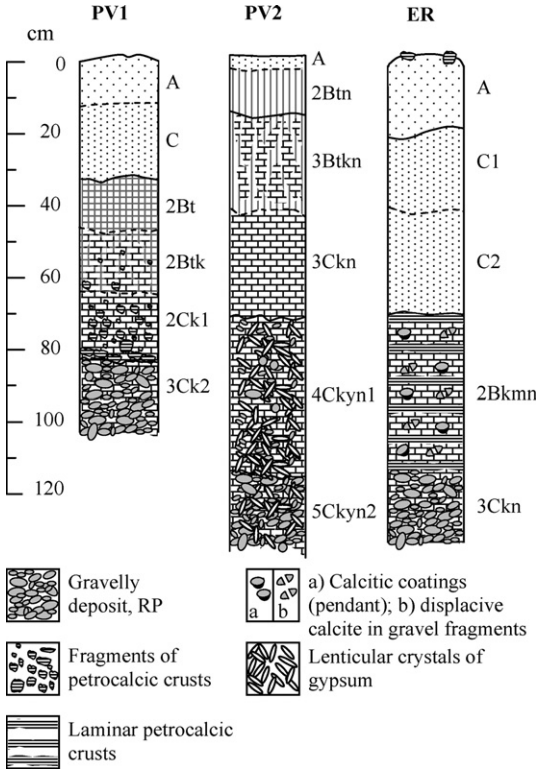

Fig. 3. Main morphological characteristics of the soil profiles studied.

The related distribution pattern c/f was open and double-spaced porphyric. The mineral grains were generally rounded and slightly altered. The coarse mineral components contained, in order of the abundance: quartz, plagioclases, K-feldspar, pyroxenes, amphiboles, opaques, and fragments of acidic volcanic rocks.

The soil formed would have been eroded and subsequently buried by sandy fine material presumably of aeolian origin, which would have evolved into the A–C horizons. The increase in depth of the Si:Al and Mg:Al molar ratios indicates the relative enrichment of Mg-silicate throughout the profile (Table 1). The PV1 soil had lower concentrations of soluble salts in the SE, with EC values of up to 1.2 dS m^{-1} in the 3Ck2 horizon (Table 2). Although the Na^+, together with the Cl^-, dominated in the SE, the ESP values did not surpass 15%, and thus the soil in PV1 was classified as Xeric Calciargid. The $H_4SiO_4^0$ concentrations in the SE varied from 0.66 to 0.27 $mmol_{(c)}\ L^{-1}$, with the highest values recorded in the upper horizons (Table 2).

In the PV2 soil, the upper part of RP (5Ckyn2 horizon), had an equivalent calcium-carbonate content of 16.4%. This horizon was buried by a sediment that contained soluble salts and gypsum. During a period of relative stability, this deposit would have been leached with the subsequent carbonate precipitation (17.7%) in the 4Ckyn1 horizon, followed by pedogenic-gypsum formation which affected the underlying calcic horizon. The presence of gypsum was also indicated by the higher Ca^{2+} and SO_4^{2-} contents in the SE (Table 2). Macromorphologically, the gypsum was detected in small crystalline aggregates with diameters of a few millimeters. In thin sections, the gypsum formed lenticular crystallitic aggregates intergrown in the micritic matrix (Fig. 4d).

The sequence of the 3Btkn-3Ckn horizons represents a new deposit in which carbonate leaching and dispersion–illuviation of clays occurred during a younger pedogenetic period. This horizon sequence has macro- and micro-morphological characteristics similar to the sequence of the 2Btk-2Ck horizons of the PV1 soil. In a new geomorphic episode, the 3Btkn-3Ckn horizons were underlined by a new saline deposit which evolved into a 2Btn horizon. In the PV2 soil, the clay dispersion through Na^+ and illuviation produced clay coatings thicker (30–100 μm) than in the Bt horizons of the PV1 soil (<30 μm). Finally, the 2Btn horizon was eroded and later was buried by a sandy material which evolved into an A horizon. Given the morphological and physico-chemical characteristics, the PV2 soil was classified as Xeric Natrigypsid.

In the PV2 soil, similar to the pV1 soil, the Mg:Al and Si:Al molar ratios also increased with depth, showing an enrichment in Mg-silicates; nevertheless, the saturation extract had higher soluble-salt contents (Table 2) where, the fluoride concentration augments in depth with values between 0.12 and 1.03 $mmol_{(c)}\ L^{-1}$, and the $H_4SiO_4^0$ contents tend to diminish from 1.3 $mmol_{(c)}\ L^{-1}$ to 0.3 $mmol_{(c)}L^{-1}$.

The ER soil was subjected to similar but more intense processes of carbonate leaching. The upper part of RP has about 13% carbonate accumulation, partially cementing the matrix of the gravel deposit constituting the 3Ckn horizon. This surface was presumably eroded and later covered by a

Table 1
Field soil data and selected properties of the soils studied

Horizon	Depth (cm)	Colour dry	Structure[a]	Boundary[a]	Gravels (%)	Sand (%)	Silt	Clay	$CaCO_3$ (%)	OC[b] (%)	Gypsum (%)	CEC ($cmol_{(c)}$ kg^{-1})	Mg:Al	Si:Al
PV1														
A	0–10	10YR6/3	gr, vf, 1	aw	1.6	74.6	14.2	11.0	0.77	1.07	nd	13.89	0.22	7.74
C	10–29	10YR6/3	sg	aw	3.9	71.2	15.9	12.9	0.03	0.57	nd	11.57	0.21	7.70
2Bt	29–38	7.5YR5/4	sbk, m, 2	ci	1.0	57.2	19.2	23.7	2.97	0.49	nd	18.90	0.44	8.11
2Btk	38–52	7.5YR7/4	sbk, m, 2	gw	3.4	55.0	7.0	38.0	14.25	0.36	nd	13.50	0.47	8.78
2Ck1	52–66	7.5YR8/2	m	ai	22.8	59.3	15.2	25.5	20.36	0.34	nd	13.58	0.50	8.90
3Ck2	>66	7.5YR8/2	m	–	74.5	53.0	5.3	41.7	26.12	0.31	nd	12.34	0.63	9.51
PV2														
A	0–2	10YR5/3	gr, vf, 1	as	0.2	85.3	11.8	2.9	0.13	0.72	nd	8.10	0.21	7.81
2Btn	2–15	10YR3/4	pr, f, 3	aw	0.4	45.9	8.4	45.6	0.17	0.86	nd	22.76	0.39	6.88
3Btkn	15–40	10YR5/3	sbk, m, 2	as	1.2	59.2	3.8	37.0	13.02	0.20	nd	14.27	0.47	8.30
3Ckn	40–65	10YR7/3	m	as	1.1	61.9	5.2	32.9	11.36	0.16	nd	14.27	0.44	8.10
4Ckyn1	65–91	10YR8/3	m	as	0.4	41.3	6.1	52.6	17.73	0.14	12	6.56	0.84	8.81
5Ckyn2	>91	10YR8/3	m	–	14.6	47.7	14.7	37.6	16.40	0.13	7	8.49	0.83	9.94
ER														
A	0–20	10YR6/3	gr, vf, 1	as	8.5	78.8	15.6	5.7	0.89	0.82	nd	14.30	0.33	8.91
C1	20–41	10YR6/3	sg	gi	14.9	78.6	14.8	6.6	4.78	0.47	nd	13.54	0.33	9.05
C2	41–68	10YR6/3	sg	ai	13.0	78.7	14.8	6.5	2.46	0.45	nd	13.54	0.34	9.21
2Bkmn	68–102	10YR8/2	pl, m, 3	aw	4.4	51.1	11.7	37.2	60.36	0.29	nd	6.02	2.35	12.77
3Ckn	>102	10YR6/3	m	–	77.8	63.3	14.6	22.1	12.82	0.19	nd	12.04	0.56	10.46

nd: not detected.
[a] Abbreviations for morphological description are from Soil Survey Staff (1999).
[b] OC: organic carbon.

deposit in which the intense carbonate leaching filled pores and formed a petrocalcic horizon (2Bkmn horizon), with an equivalent carbonate content of about 60%. This horizon was composed of a hard massive layer, in which platy laminar crusts of 2–3 cm thick were found to be intercalated (Fig. 3). The molecular ratios Mg:Al and Si:Al proved higher in the calcretized zone of the ER profile, principally in the petrocalcic horizon (Table 1).

Macroscopically, calcitic coatings on gravels (pendant type) and evidence of displacive growth of calcite was detected,

Table 2
Chemical composition of soil solutions from saturation extracts (SE)

Horizon	Reference	pH	EC (dS m^{-1})	Ca^{2+}	Mg^{2+}	Na^{+}	K^{+}	Cl^{-}	F^{-}	HCO_3^{-}	SO_4^{2-}	$H_4SiO_4^0$	ESP (%)
				($mmol_{(c)}$ L^{-1})									
PV1													
A	1	8.07	0.72	1.99	1.35	1.65	0.53	1.66	0.11	1.65	1.44	0.66	0.62
C	2	8.12	0.53	0.65	1.10	2.12	0.34	0.70	0.12	2.83	0.77	0.63	2.03
2Bt	3	8.01	1.05	1.36	1.82	5.87	0.44	4.26	0.24	1.90	2.18	0.54	5.31
2Btk	4	7.63	1.04	0.99	1.58	6.10	0.57	5.29	0.26	1.50	1.55	0.37	6.25
2Ck1	5	7.58	1.01	0.67	1.28	6.81	0.50	4.81	0.12	2.50	1.44	0.27	8.18
3Ck2	6	8.45	1.16	0.90	1.92	10.17	0.63	9.34	0.13	2.40	1.86	0.29	10.21
PV2													
A	7	7.98	0.99	2.36	1.58	2.75	0.82	1.75	0.12	3.84	2.18	0.53	1.60
2Btn	8	8.10	1.50	0.59	1.15	14.31	0.44	8.24	0.26	7.41	1.97	1.27	17.59
3Btkn	9	7.85	6.97	2.93	6.94	119.90	1.99	112.66	0.54	1.79	20.94	0.33	43.93
3Ckn	10	8.01	8.44	5.86	15.97	168.31	1.18	182.26	0.99	1.15	29.03	0.31	42.49
4Ckyn1	11	7.48	7.88	15.14	24.36	163.76	1.18	179.87	1.00	0.82	43.71	0.26	34.68
5Ckyn2	12	7.51	7.40	14.16	22.91	154.99	1.33	168.89	1.03	0.66	42.97	0.29	34.14
ER													
A	13	7.71	0.71	4.20	0.90	1.97	1.07	0.96	0.12	6.55	1.28	0.56	0.55
C1	14	7.81	0.59	3.17	0.46	3.42	0.19	1.00	0.13	6.32	1.29	0.61	2.42
C2	15	7.57	1.23	3.04	0.54	12.74	0.07	2.71	0.26	8.63	4.50	0.71	11.33
2Bkmn	16	8.28	2.80	1.39	0.53	29.77	0.17	26.07	0.95	5.71	4.72	0.89	30.35
3Ckn	17	8.08	4.24	1.70	0.48	52.93	0.17	43.18	1.59	1.65	15.27	0.65	42.41

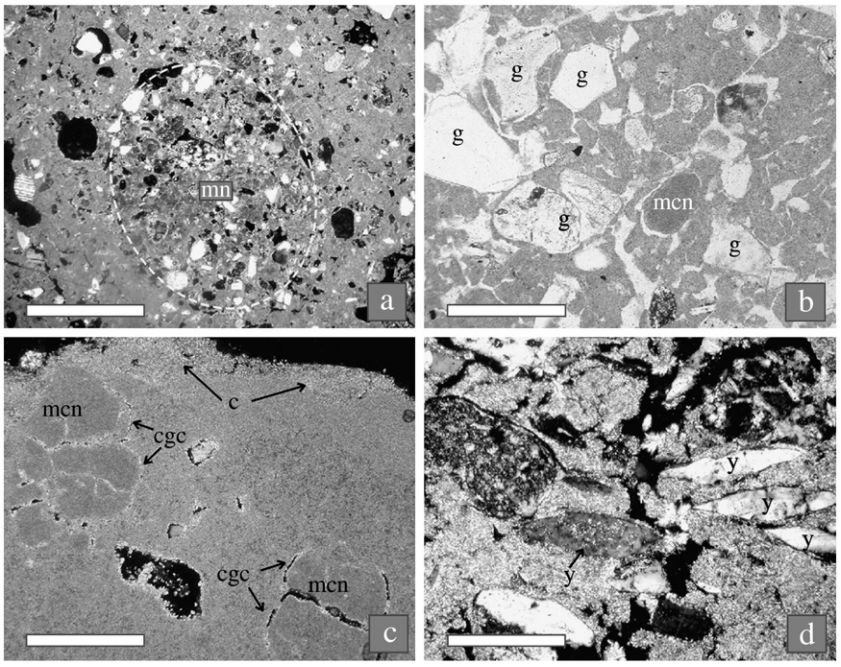

Fig. 4. Features of alpha-type microstructure. PPL: plane polarized light. XPL: crossed polarized light; a) 3Ck2 horizon of PV1 soil: rounded matrix nodule (mn), dense micritic micromass and floating mineral grains, bar scale = 500 μm. XPL; b) coarse mineral components (g) and micritic calcite nodules (mcn) are surrounded by circum-granular cracks; bar scale = 200 μm. PPL; c) petrocalcic crust fragment: dense micritic micromass. Micritic calcite nodule (mcn) with circum-granular crack (cgc) and subsequent calcite crystallization (c), bar scale = 300 μm. XPL; d) 4Ckyn1 horizon of PV2 soil: crystal intergrowths of lenticular gypsum (y), bar scale = 150 μm. XPL.

where the calcitic matrix separated the gravels and fragmented them. The calcic and petrocalcic horizons in the ER soil had higher soluble-salt contents than did the overlying horizons (Table 2), where the Na^+ and Cl^- ions were dominant. The ESP was >15%, and hence these horizons (2Bkmn-3Ckn horizons) acquired a natric character. The F^- concentration ranged from 0.95 to 1.59 $mmol_{(c)}\ L^{-1}$ and in the 2Bkmn horizon the higher values of $H_4SiO_4^0$ and pH were determined (Table 2).

Table 3
Mineral distribution of the soils studied

Horizon	Bulk samples (powder XRD)							Clay fraction (oriented aggregates)							
	Q	Pl	Fk	Phyll	Calc	Gy	Fl	Sp	P	S	I	K	Q	Pl	Fl
PV1															
A	++	+++	+	++	nd	nd	nd	nd	nd	+	+++	(+)	++	+	nd
C	++	+++	+	++	nd	nd	nd	nd	nd	+	+++	+	+	+	nd
2Bt	++	++	+	+++	+	nd	nd	nd	nd	++	++	+	+	+	nd
2Btk	++	+	+	++	++	nd	nd	nd	nd	++	++	+	+	+	nd
2Ck1	++	++	+	++	++	nd	nd	nd	nd	++	++	+	+	+	nd
3Ck2	++	++	+	++	++	nd	nd	nd	+++	+	++	+	+	+	nd
CF								+++	++	(+)	+	(+)	(+)	(+)	nd
PV2															
A	++	+++	nd	nd	nd	nd	nd	nd	nd	+	++	+	++	++	nd
2Btn	++	++	+	+++	nd	nd	nd	nd	nd	+	+++	+	+	+	nd
3Btkn	++	+	+	++	++	nd	nd	nd	nd	+++	++	+	+	+	nd
3Ckn	++	++	nd	++	++	nd	nd	nd	nd	+++	++	+	+	+	nd
4Ckyn1	+	+	nd	++	++	++	nd	nd	+++	+	(+)	(+)	+	+	nd
5Ckyn2	+	+	nd	++	++	++	nd	nd	+++	++	(+)	(+)	+	+	nd
ER															
A	+++	++	nd	nd	+	nd	nd	nd	nd	++	++	+	++	+	nd
C1	++	+++	nd	++	+	nd	nd	nd	nd	++	++	+	++	+	nd
C2	++	++	nd	++	+	nd	nd	nd	nd	++	++	+	++	++	nd
2Bkmn	++	(+)	nd	+	+++	nd	(+)	+++	++	+	(+)	nd	(+)	+	+
3Ckn	++	++	+	++	++	nd	nd	nd	++	++	++	(+)	+	++	nd

Q: quartz; Fk: potassic feldspar; Pl: plagioclase; Phyll: phyllosilicates; Calc: calcite; Gy: gypsum; Fl: fluorite; Sp: sepiolite; P: palygorskite; S: smectite; I: illite: K: kaolinite; nd: not detected; (+): traces; +: 5–10%; ++: 15–40%; +++: >40%. CF: calcrete fragment.

Geomorphic processes would have truncated the soil surface, exhuming the thick and hard petrocalcic horizon, which was buried by sandy material of presumably aeolian origin producing a A-C1-C2 horizon sequence. These horizons had a loose consistency with no structure (single grains), and only the A horizon had a weak, very fine granular structure. The equivalent carbonate contents in these horizons were between 0.9 and 4.8%; this was due to the presence of calcitic pseudo-sand grains, coming from the of an old calcic horizon. The ER soil was classified as Xeric Petrocalcid.

3.2. Soil mineralogy

The powder XRD diagram indicates the presence of quartz, feldspar, phyllosilicate, calcite and gypsum (Table 3). As can be seen in Fig. 5 the 3.03 Å (104) peak indicates the presence of low-Mg calcite (Goldsmith and Graf, 1958). In the 2Bkmn horizon of the ER profile, low peaks in 3.145 Å, 1.93 Å, and 1.65 Å were attributed to fluorite (Fig. 5).

The clay fraction has a mixture of minerals formed by: illite, interstratified illite–smectite, smectite, kaolinite, palygorskite, and sepiolite (Table 3 and Fig. 6). Accessory minerals were quartz and plagioclases. Illite was identified by its characteristic peak of 10.0 Å (001) and 5.0 Å (002). This mineral predominates in the A–C horizons of the PV1 soil and A-2Btn horizons of the PV2 soil. In these horizons, smectites have very diffuse peaks in a wide range of reflections, forming a plateau together with the irregular interstratified 2:1 minerals and illite (Fig. 6). In the A-C1-C2 horizons of the ER soil the illite:smectite ratio was about 1.

The XRD pattern depicted in Fig. 6 shows that the 2Bt-2Btk-2Ck1 horizons of the PV1 soil and the 3Btkn-3Ckn horizons of the PV2 soil, have well-defined peaks in the 14–15 Å (001) region, which expand after being treated with ethylene glycol to 16–18 Å, indicating the predominance of smectites. Traces of kaolinite were found in the deepest horizons.

The XRD patterns of the 3Ck2 horizon of the PV1 soil, the 4Ckyn1-5Ckyn2 horizons of the PV2 soil, and the 3Ckn horizon of the ER soil (Fig. 6), showed smectite and strong peaks at 10.6 Å (110) as well as moderate lines in the 6.4 Å (200) region, which does not expand on ethylene glycol treatment, indicating the presence of palygorskite.

In the 2Bkmn horizon of the ER soil and in fragments of the petrocalcic crusts included in the 2Ck1 horizon of the PV1 soil, sepiolite was identified as the dominant clay mineral together with palygorskite. This conclusion was based on the presence of strong peaks at 12.2 Å (110) and moderate peaks at 4.4 Å (131). The moderate XRD lines at 3.34 Å, corresponding to sepiolite, could overlap with the strong peak of quartz. In the 2Bkmn horizon of the ER soil, fluorite was identified by three clear and quite intense peaks of 3.15 Å, 1.93 Å, and 1.65 Å (Fig. 6).

The presence of fibrous minerals in the soils studied was confirmed by the typical morphology observed through the SEM. Fig. 7a–b corresponds to the clay fraction of the 3Ck2 horizon of the PV1 profile, where a chaotic (anarchic) occurrence

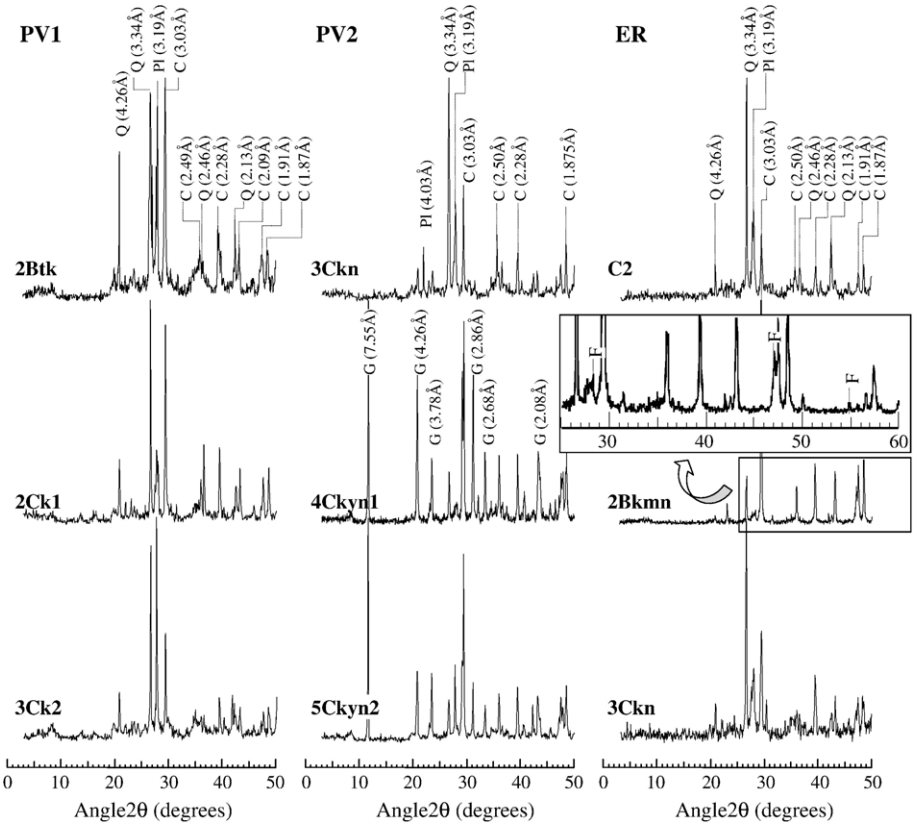

Fig. 5. Powder XRD diagrams on bulk samples from calcic, calcic-gypsic and petrocalcic horizons; Q: quartz; Pl: plagioclase; C: calcite; G: gypsum; F: fluorite.

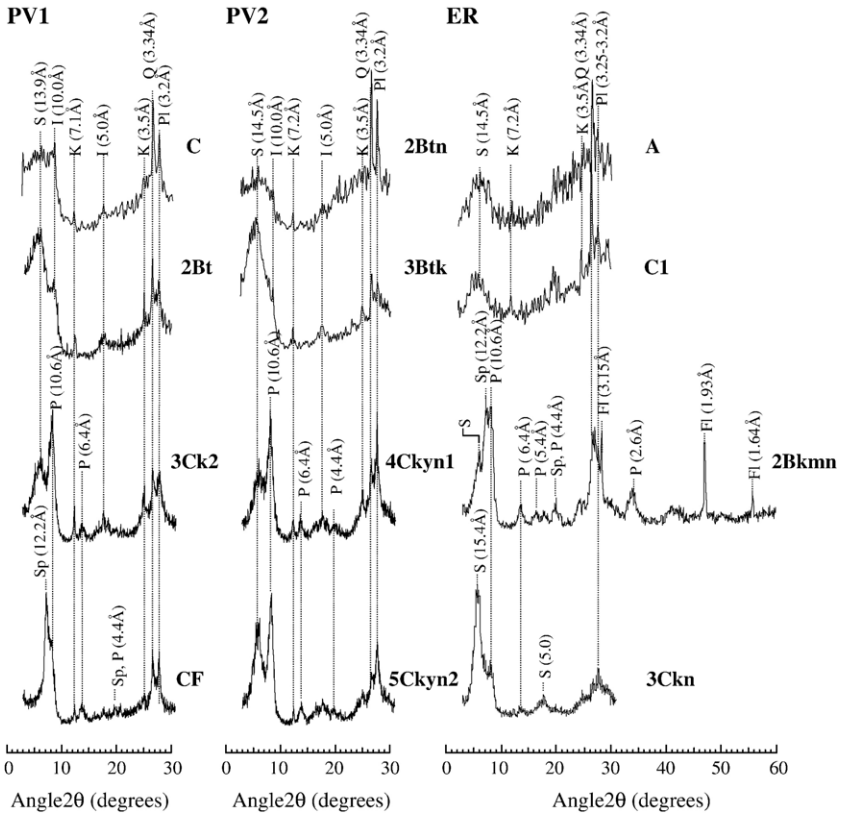

Fig. 6. X-ray diffractograms on clay fraction from selected horizons; Q: quartz; Pl: plagioclase; Fl: fluorite; Sp: sepiolite; P: palygorskite; S: smectite; I: illite; K: kaolinite. CF: calcrete fragment.

of palygorskite fibers as laths up to 1 μm long and 0.1 μm wide were detected. In the 2Bkmn horizon of the ER profile, sepiolite was observed in planar aggregates, the fibers of which (up to 3 μm long and 0.1 μm wide) had curved and frayed ends (Fig. 7c). Rounded equi-dimensional aggregates, intergrowth in sepiolite fibers, were also visible (Fig. 7d). The average diameter of these aggregates was about 1 μm, formed by poorly defined micro-crystals.

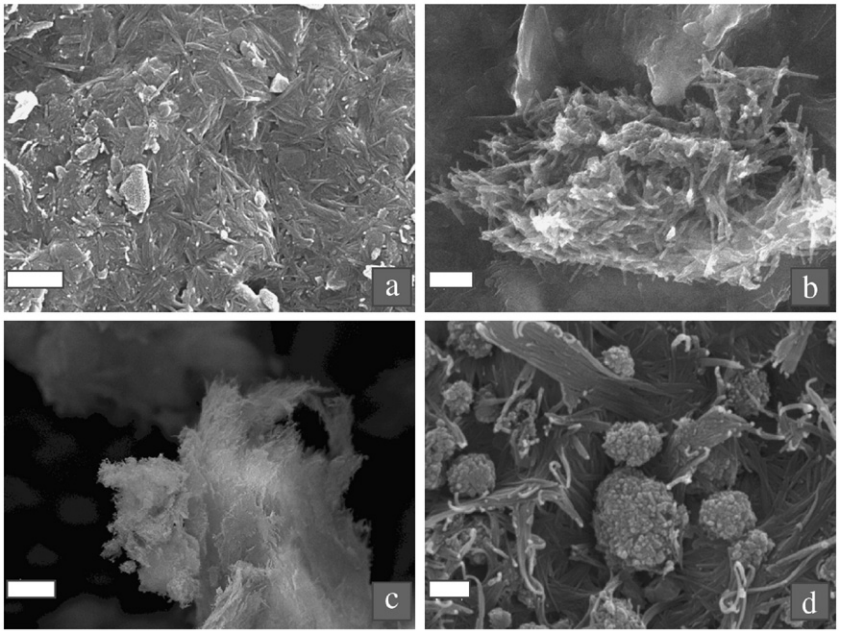

Fig. 7. SEM morphologies of fibrous clay; a) a chaotic disposition of palygorskite micro-fibers from 3Ck2 horizon of PV1 soil, bar scale = 1 μm; b) detail of the Fig. 7a, bar scale = 0.5 μm; c) cluster of sepiolite fibers from 2Bkmn horizon of ER soil, bar scale = 5 μm; d) details of c-scanning electron micrograph: planar aggregate of micro-fibers, the ends of which are curved and spherules of micro-crystal aggregates, bar scale = 0.5 μm.

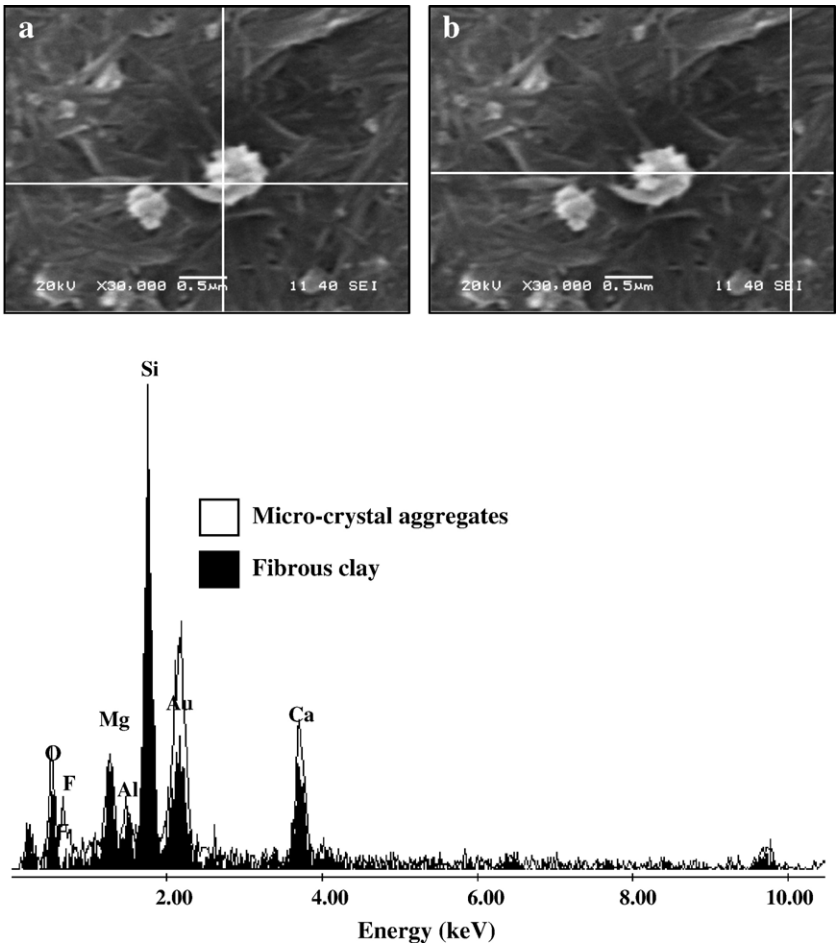

Fig. 8. SEM images and EDS spectrums on a) micro-crystal aggregates and on b) fibrous-clay matrix.

The micro-crystal aggregates and matrix of fibrous clay were analyzed in the SEM-EDS, and a spectrum was shown in Fig. 8. The semi-quantitative elemental analysis on five different observations of a fibrous-clay matrix and micro-crystal aggregates support the occurrence of Mg-hydroxy-silicate (Table 4). This analysis also revealed that the micro-crystal aggregates had higher F contents than in the matrix of fibrous clay, which is attributed to fluorite identified in XRD (Fig. 6). An aspect to consider is the spatial resolution of the electron beam (with accelerating voltage of 20 kV), which was about 1 μm, and thus an interaction volume of 1 μm^3 was analyzed. Thus, the semi-quantitative analysis of aggregates can be influenced by the interaction with the neighboring fibrous-clay matrix. The relatively higher Ca content in the fibrous-clay matrix was due to carbonate impurity and this was likely due to the incomplete removal with Na-acetate buffer solution.

Table 4
Elemental analysis through energy-dispersive X-ray fluorescence (EDS) of the 2Bkmn horizon, ER soil; numbers represent five different determinations

		O		F		Mg		Al		Si		Ca	
		Wt	At	Wt	At	Wt	At	Wt	At	Wt	At	Wt	At
		(%)											
Fibrous-clay matrix	1	32.9	47.7	6.9	8.5	11.6	11.1	1.8	1.6	14.5	12.1	32.3	18.8
	2	37.7	53.6	2.5	3.0	12.1	11.3	3.0	2.6	17.4	14.1	27.3	15.5
	3	47.9	60.5	9.3	9.9	12.6	10.4	2.1	1.6	16.2	11.7	11.9	6.0
	4	36.3	50.2	4.1	4.7	10.0	9.1	2.8	2.3	32.9	25.9	14.1	7.8
	5	31.4	45.0	3.0	3.7	11.4	10.7	4.5	3.8	34.2	28.0	15.6	8.9
Micro-crystal Aggregates	1	5.5	9.1	25.8	36.2	11.1	12.2	2.9	2.8	11.7	11.1	43.1	28.6
	2	29.5	40.9	25.2	29.4	6.4	5.8	1.7	1.4	8.3	6.5	28.9	16.0
	3	39.5	51.0	21.4	23.3	9.1	7.7	1.4	1.1	9.5	7.0	19.2	9.9
	4	34.2	46.4	13.3	15.2	9.4	8.4	3.3	2.7	24.6	19.1	15.2	8.2
	5	28.6	39.5	17.6	20.5	9.6	8.7	4.3	3.5	24.7	19.5	15.2	8.4

4. Discussion

4.1. Soil diagnostic characteristics

Since the RP is free of carbonates and since the Ca^{2+} released during weathering is not adequate to explain the $CaCO_3$ content in the soils, this mineral must have an allochthonous origin, either aeolian (Vogt and del Valle, 1994) or from runoff. In any case, these carbonates were likely redistributed in the soils. The calcic and petrocalcic horizons that developed on the RP soil have an *in situ* (pedogenic) origin. This can be easily recognized macroscopically in the 2Bkmn horizon of the ER soil by the calcitic coatings of pendant type and the displacive growth of calcite in gravels. The pedogenic origin was confirmed by thin-section analysis in the calcic horizon of the PV1 and PV2 soils.

The presence of mineral grains and micritic calcite nodules surrounded by circum-granular cracks, together with the floating mineral grains in the crystallitic b-fabric micro-mass, would indicate an *alpha*-type micro-structure (physico-chemical origin) and displacive calcite crystallization by evaporation from supersaturated soil solution (Wright, 1990; Jacks and Sharma, 1995). The precipitation of the micritic low-Mg calcite would indicate a fast evaporation from supersaturated solutions (Watts, 1978) and an increase in the Mg/Ca relationship in the soil solution. The resulting increase in the ionic activity of Mg^{2+} favors the formation of fibrous clays (Watts, 1980). As with calcite, the lenticular crystals of pedogenic-gypsum precipitation in the 4Ckyn-5Ckyn horizons of the PV2 soil, caused a displacement of the micritic matrix, due to the force of crystallization (Fig. 4d). The presence of lenticular gypsum could also indicate a quick evaporation of the soil solution during dry season (Watson, 1985).

The soluble salts appear to have an aeolian origin and would come from the marine sedimentites, the Puerto Madryn Formation, and from the salt flats in the closed basins (salines), at the time that they were redistributed later in the soil profiles (Bouza et al., 2005).

4.2. Mineralogy and soil evolution

The surface and sub-surface horizons, i.e. A–C of the PV1 soil, A-2Btn of the PV2 soil, and A-C1-C2 of the ER soil, present the beginning of illite alteration. Under conditions of pMg = 3.3–3.8, pH_4SiO_4 = 2.9–3.3, and pH = 7.7–8.1, the instability of illite is determined by a low activity of the K^+ (pK = 3 to 4; Lindsay, 1979). Under these conditions, illite is altered, where K^+ ions are exchanged by hydrated Mg^{2+} ions to form smectite (Jackson, 1964). These horizons have Mg:Al molar ratios of between 0.2 to 0.3 and Si:Al of 6.9 to 9.2.

An older pedogenic episode would correspond to the horizon sequences of the 2Bt-2Btk-2Ck1 of the PV1 soil and the 3Btkn-3Ckn of the PV2 soil, where the alteration of illite to smectite was more advanced (Fig. 6). This greater transformation to smectite is also demonstrated by an enrichment in Mg-silicates, with a Mg:Al and Si:Al molar ratios of 0.4–0.5 and 8.1–8.9, respectively.

The palygorskite is closely related to the development of calcic horizons, with a calcium-carbonate content between 13 and 26% and an increase in the molar ratios of Mg:Al (0.6–0.8) and Si:Al (8.8–10.4). Appearance of the palygorskite fibers resembles that reported by López Galindo and Viseras Iborra (2000) and Jamoussi et al. (2003). The palygorskite occurred in the textural transition between the fine materials of the calcic horizons and the coarsest deposits of the RP, 3Ck2 of PV1, 4Ckyn-5Ckyn of PV2 and 3Ckn of ER soils. A similar situation is described by Yaalon and Wieder (1976) in Calcids from Israel, where the palygorskite concentration is favored by temporary waterlogging when the infiltration water accumulates at the boundary between horizons of contrasting textures. This occurs when the infiltrated water is retained before reaching the necessary pressure to fill the largest pores of the underlying horizon. In addition, a clear relationship between the decrease of smectite and increase of palygorskite content can be seen (Table 3 and Fig. 6), and this has been used to indicate a smectite→palygorskite transformation (Yaalon and Wieder, 1976).

The occurrence of sepiolite in the 2Bkmn horizon of the ER profile and in fragments of petrocalcic crusts incorporated in the 2Ck1 horizon of the PV1 profile, suggests that this mineral is strongly related to a greater advance of calcretization. The planar or sheet aggregates of sepiolite (and associated palygorskite) fibers with curved and frayed ends, are comparable to the ones described by Singer et al. (1995) and Singer (1989, 2002). In the 2Bkmn horizon of the ER soil, the higher molar ratios of Mg:Al (2.4) and Si:Al (12.8) were recorded, indicating an enrichment in fibrous-clay minerals. This is also supported by the low CEC values (Table 1).

The petrocalcic crust fragments with sepiolite in the 2Ck1 horizon of the PV1 soil would indicate a previous pedogenic event. These fragments may have been transported by water erosion from petrocalcic horizons of the oldest and most elevated levels of the RP soils.

To evaluate whether the present soil environment is favorable to smectite–palygorskite–sepiolite stability, we plotted the chemical compositions of the SE on a mineral-stability diagram (Fig. 9), as proposed by Jones and Galán (1988), which is based on the following reactions:

$$5\text{palygorskite} + 15.6\text{pH} + 24.4H_2O = 3\text{smectite} + 7.65Mg^{2+} + 15.6H_4SiO_4^0, \quad (1)$$

$$\log K_{\text{paly}-\text{smect}} = \log Mg^{2+} + 2\text{pH} + 2\log H_4SiO_4^0 = 5.75$$

(Weaver and Beck, 1977) and

$$Mg_2Si_3O_6(OH)_4(\text{sepiolite}) + 2H_2O + 4H^+ = 2Mg^{2+} + 3H_4SiO_4^0 \quad (2)$$

$$\log K_{\text{sepiolite}} = \log Mg^{2+} + 2\text{pH} + 1.5\log H_4SiO_4^0 = 7.945$$

(Lindsay, 1979)

The calcic 3Ck2 horizons of the PV1 and 3Ckn of the ER soil enriched with palygorskite fall within the palygorskite stability field. However, the data of the 4Ckyn1-5Ckyn2 horizons of the

PV2 soil fall on the boundary line. The 2Bkmn horizon of the ER soil enriched with sepiolite, however, falls within the stability field of this clay mineral.

Some surface and sub-surface horizons with predominant smectite, illite, and interstratified illite–smectite fall within the palygorskite–sepiolite stability fields, but the reason for this is not well understood and deserves a more detailed study (Fig. 9). The use of equilibrium diagrams shows the tendency towards a more stable mineral phase, in which kinetic factors must be considered, because the rates of precipitation and dissolution of minerals are often so low that true equilibrium is not reached (Lindsay, 1979; Smeck et al., 1983).

This situation of non-equilibrium was observed by Monger and Daugherty (1991), who concluded that a soil-water extract prepared for 24 h could not reflect the pedochemical history of an ancient soil. Singer et al. (1995) reported similar results, suggesting that the clay minerals are in an alteration/transformation state within other mineral phases caused by climatic changes during the Quaternary. If palygorskite and sepiolite are the stable end products, these would require the time necessary to reach equilibrium, but also a confined environment and calcretization processes that control the Mg–Si–pH equilibrium.

The palygorskite–sepiolite association would indicate that during low-Mg calcite precipitation, the activity of Mg^{2+} would have been sufficient for the transformation smectite → palygorskite to the point that, in a more advanced stage of calcretization, palygorskite reduces available aluminum while sepiolite is precipitated (Watts, 1980). This clay–mineral sequence indicates some time dependency for formation, which was found, for example, by Bachman and Machette (1977) in Aridisols from the east of the United States and by Watts (1980) in calcretes of the semi-arid region of Southern Africa.

The Mg^{2+}:$H_4SiO_4^0$ ratio in the 2Bkmn horizon of the ER soil is <2/3 (Table 2) and, according to Eq. (2), the soluble silica would be in excess and could precipitate as opal-CT during evaporation. The opal-CT nodules are a common feature in calcretes with sepiolite (Hay and Wiggins, 1980), and are generally found in the spherules of micro-crystal aggregates. However, opal-CT must have been in low amounts since it was not detected in the XRD patterns.

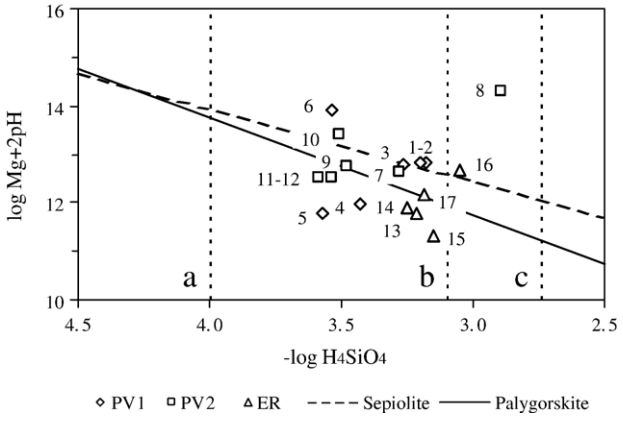

Fig. 9. Stability diagram for sepiolite–palygorskite–smectite system and plotted composition (activities) of soil-water extracts of soil horizons (reference to see Table 3). Saturation solubility of SiO_2: a) quartz, b) soil SiO_2, c) amorphous SiO_2.

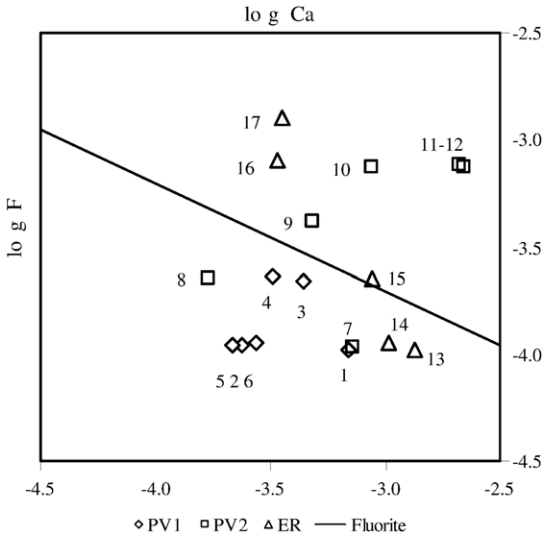

Fig. 10. Fluorite-stability diagram and plotted fluoride and calcium chemical activities of soil-water extracts (reference to see Table 3).

On the other hand, although in the calcic horizons of the PV2 and ER soils the ionic activities of Ca^{2+} and F^- reached equilibrium with respect to the fluorite (Fig. 10), only in the 2Bkmn horizon of the ER soil did it precipitate in sufficient amounts to be detected by XRD (Fig. 6). In this sense, the micro-crystal aggregate intergrowth among sepiolite fibers shown in Fig. 7c and analyzed in SEM-EDS (Fig. 8 and Table 4), would correspond to spherules of fluorite and opal-CT; meanwhile the fluorine identified in the fibrous-clay matrix (Fig. 8 and Table 4), could correspond to F^- ions in the OH^- position of the sepiolite (Santaren et al., 1990; Jacks et al., 2005).

The association of calcite, fluorite, sepiolite, and opal-CT would indicate a successive precipitation of these minerals and an alkalinization mechanism during the evaporation processes (Jacks and Sharma, 1995; Barbiéro and Van Vliet-Lanoe, 1998; Chernet et al., 2001). These precipitations sequester divalent cations from the soil solution, thereby increasing the relation $Na^+/(Ca^{2+}+Mg^{2+})$ and thus the ESP (Table 2).

5. Conclusions

The study of soil-geomorphology relationships provides a new opportunity to advance our knowledge of the genesis of palygorskite and sepiolite in soils of Argentina and South America. The clay mineralogy is related to the age of the pedogenic episodes that affected the geomorphic surfaces studied. From younger to older pedogenetic episodes, the clay-mineralogical properties were:

1) In the superficial and sub-superficial horizons, A–C horizons of the Calciargid and Petrocalcid and A-2Btn horizons of the Natrigypsid, illite was the predominant and inherited clay mineral of the parent material. This clay

mineral was slightly altered to interstratified illite–smectite and smectite due to the exchange of K^+ by hydrated Mg^{2+} from the soil solution.

2) In the argillic and calcic horizons, corresponding to the 2Bt-2Btk-2Ck1 horizons of the PV1 soil and 3Btkn-3Ckn horizons of the PV2 soil, the alteration illite → smectite was more progressive and therefore smectite was the most abundant in the fraction <2 μm.
3) In the calcic and calcic-gypsic horizons that are at the upper limit of the RP (3Ck2 horizon of the PV1 soil, 4Ckyn1-5Ckyn2 horizons of the PV2 soil, and 3Ckn horizon of the ER soil), palygorskite was the predominant clay mineral and was associated with smectite. These horizons had an *alpha*-type micro-structure and a displacive calcite growth by evaporation from supersaturated soil solutions. The carbonate was mainly low-Mg calcite and, during its precipitation, the Mg^{2+} activity must have increased in the soil solution, favoring the smectite → palygorskite transformation. These pedogenic processes were confirmed by the magnesium, pH, and soluble silica activity diagram. The soil environment, favorable for this transformation, was the textural transition between the fine materials of sub-surface horizons and the coarsest deposit of RP, where temporary waterlogging occurred.
4) In the mature calcrete corresponding to 2Bkmn horizon of the ER soil and re-transported fragments of petrocalcic crust included into calcic horizon of the PV1 soil, sepiolite was the predominant clay mineral. During the calcretization processes, the sepiolite precipitated from the soil solution after the palygorskite formation.
5) The fluorite was identified by XRD and SEM-EDS in the petrocalcic horizon and its pedogenetic origin was also corroborated through the chemical composition of the soil solution.
6) The association of calcite, fluorite, sepiolite (Mg-hydroxy-silicates), and possibly opal-CT, indicates a successive precipitation of these minerals under alkaline conditions during the evaporation processes.

Acknowledgments

This study was partially supported by FONCyT Project N° PICT98-07-04094 (Agencia Nacional de Promoción Científica y Técnica, Argentina) and Project PIP N° 6479, CONICET, Argentina. XRD analyses, thin sections and SEM observations were made through the Department of Pedology of the University of Granada (Science Faculty). The authors thank ALUAR (Aluminio Argentino S.A.I.C.) for permission to use the SEM-EDS and to Mr. Jaime Groizard for assistance with the equipment. The authors thank Dr. A.R. Mermut and to an anonymous reviewer for their suggestions for improving this manuscript.

References

Abtahi, A., 1977. Effect of a saline and alkaline ground water on soil genesis in semi-arid southern Iran. Soil Science Society of America Journal 41, 583–588.

Bachman, G.O., Machette, M.N., 1977. Calcic soils and calcretes in the southwestern United States. U.S.Geol. Surv. Open-File Report, pp. 77–794.

Barahona, E., 1974. Arcillas de ladrería de la provincia de Granada: evaluación de algunos ensayos de materias primas. Tesis Doctoral, Universidad de Granada, Granada, Spain.

Barbiéro, L., Van Vliet-Lanoe, B., 1998. The alkali soils of the middle Niger valley: origins, formation and present evolution. Geoderma 84, 323–343.

Birkeland, P., 1984. Soil and Geomorphology. Oxford University Press, New York.

Bouza, P., Simón, M., Aguilar, J., Rostagno, M., del Valle, H., 2005. Genesis of some selected soils in the Valdés Peninsula, NE Patagonia, Argentina. In: Faz Cano, A., Ortiz, R., Mermut, A. (Eds.), Advances in Geo Ecology, vol. 36. Catena Verlag GMBH, Reiskirchen, pp. 1–12.

Brock, A.L., Buck, B.J., 2005. A new formation process for calcic pendants from Pahranagat Valley, Nevada, USA, and implication for dating Quaternary landforms. Quaternary Research 63, 359–367.

Bullock, P., Fedoroff, N., Jongerius, A., Stoops, G., Tursina, T., Babel, U., 1985. Handbook for Soil Thin Section Description. Waine Research Publications, Wolverhampton.

Chernet, T., Travy, Y., Valles, V., 2001. Mechanism of degradation of the quality of natural water in the Lake Regions of the Ethiopian Rift Valley. Water Research 35 (12), 2819–2832.

Coudé-Gaussen, C., 1987. Observation au MEB de fibres de palygorskite transportée en grains par le vent. In: Federoff, N., Bresson, L.M., Courty, M.A. (Eds.), Micromorphologie des Sols. Association Française pour l´ Étude du Sol, Paris, pp. 199–205.

del Valle, H., Beltramone, C., 1987. Morfología de las acumulaciones calcáreas en algunos paleosuelos de Patagonia oriental (Chubut). Ciencia del Suelo 5 (1), 77–87.

Elprince, A.M., Mashhady, M.S., Aba-Husayn, M.M., 1979. The occurrence of pedogenic palygorskite (attapulgite) in Saudi Arabia. Soil Science 128, 211–218.

Gee, G.W., Bauder, J.W., 1986. Particle-size analysis. In: Klute, A. (Ed.), Methods of Soil Analysis, Part 1. Physical and Mineralogical Methods. 2nd Agronomy, vol. 9. Soil Sci. Soc. Am., Madison, pp. 383–411.

Goldsmith, J.R., Graf, D.L., 1958. Relations between lattice constants and composition of the Ca–Mg carbonates. American Mineralogist 43, 84–101.

Haller, M., 1981. Descripción Geológica de la Hoja 43 h - Puerto Madryn, Provincia del Chubut. Boletín, vol. 184. Servicio Geológico Nacional, Buenos Aires.

Haller, M., Monti, A., Meister, C., 2001. Hoja Geológica 4363-1, Península Valdés, Provincia del Chubut. Boletín N° 266. Secretaría de Energía y Minería, Servicio Geológico Minero Argentino, Buenos Aires.

Hallmark, C.T., Wilding, L.P., Smeck, N.E., 1982. Silicon. In: Page, A.L., Miller, R.H., Keeny, D.R. (Eds.), Methods of Soil Analysis, Part 2. Chemical and Microbiological Properties. 2nd Agronomy, vol. 9. Soil Sci. Soc. Am., Madison, pp. 263–273.

Hay, R.L., Wiggins, B., 1980. Pellets, ooids, sepiolite and silica in three calcretes of the southwestern United States. Sedimentology 27, 559–576.

Jacks, G., Sharma, V.P., 1995. Geochemistry of calcic horizons in relation to hillslope processes, southern India. Geoderma 67, 203–214.

Jacks, G., Bhattacharya, P., Chaudhary, V., Singh, K.P., 2005. Controls on the genesis of same high-fluoride groundwaters in India. Applied Geochemistry 20, 221–228.

Jackson, M.L., 1964. Chemical composition of soil. In: Bear, F.E. (Ed.), Chemistry of the soil. Reinhold Publ. Corp., New York, pp. 71–141.

Jamoussi, F., Ben Aboud, A., López-Galindo, A., 2003. Palygorskite genesis through silicate transformation in Tunisian continental Eocene deposits. Clay Minerals 38, 187–199.

Jones, B.F., Galán, E., 1988. Sepiolite and palygorskite. In: Bailey, S.W. (Ed.), Hydrous Phyllosilicates. Reviews in Mineralogy, vol. 16. Mineralogical Society of America, pp. 631–674.

Khademi, H., Mermut, A.R., 1998. Source of palygorskite in gypsiferous Aridisols and associated sediments from Central Iran. Clay Minerals 33, 561–578.

Khademi, H., Mermut, A.R., 1999. Submicroscopy and stable isotope geochemistry of carbonates and associated palygorskite in selected Iranian aridisols. European Journal of Soil Science 50, 207–216.

Lindsay, W.L., 1979. Chemical Equilibria in Soils. John Wiley & Sons, New York.

López Galindo, A., Viseras Iborra, C., 2000. Pharmaceutical application of fibrous clay (sepiolite and palygorskite) from some circum-Mediterranean deposits. Proceeding 1st Latin American Clay Conference, Funchal, vol. 1, pp. 258–270.

Mercer, J.H., 1976. Glacial history of southernmost South America. Quaternary Research 6, 125–166.

Monger, H.C., Daugherty, L.A., 1991. Neoformation of palygorskite in a southern New Mexico Aridisol. Soil Science Society of America Journal 55, 1646–1650.

Morrás, H., Robert, M., Bocquier, G., 1981. Presencia de arcillas fibrosas pedogeneticas en suelos halomórficos de la provincia de Santa Fe. VIII Congreso Geológico Argentino. San Luis, Argentina. Actas, vol. IV, pp. 353–360.

Morrás, H., Robert, M., Bocquier, G., 1982. Caractérisation minéralogique de certains sols salsodiques et planosoliques du "Chaco Deprimido" (Argentine). Cah.O.R.S.T.O.M., sér. Pédol., vol. XIX, No 2, pp. 151–169.

Paquet, H., Millot, G., 1973. Geochemical evolution of clay minerals in the weathered products in soils of Mediterranean climate. In: Serratosa, J.M. (Ed.), Proc. Int. Conf. 1972. Madrid, pp. 199–206.

Pimentel, N.L.V., 2002. Pedogenic and early diagenetic processes in Palaeogene alluvial fan and lacustrine deposits from the Sado Basin (S Portugal). Sedimentary Geology 148, 123–138.

Santaren, J., Sanz, J., Ruiz-Hitzky, E., 1990. Structural fluorine in sepiolite. Clays and Clay Minerals 38, 63–68.

Schultz, L.G., 1964. Quantitative interpretation of mineralogical composition from X-ray and chemical data for the Pierce Shale. Professional Paper - United States Geological Survey 391-C.

Singer, A., 1989. Palygorskite and sepiolite group minerals. In: Dixon, J.B., Weed, S.B. (Eds.), Minerals in Soil Environments. Soil Sci. Soc. Am., Madison, pp. 829–872.

Singer, A., 2002. Palygorskite and sepiolite. In: Dixon, J.B., Schulze, D.G. (Eds.), Soil Mineralogy with Environmental Applications. SSSA Book Series, vol. 7. Soil Science Society of America, Madison, WI, pp. 555–583.

Singer, A., Norrish, K., 1974. Pedogenic palygorskite occurrences in Australia. American Mineralogist 59, 508–517.

Singer, A., Kirsten, W., Bühmann, C., 1995. Fibrous clay minerals in the soils of Namaqualand, South Africa: characteristics and formation. Geoderma 66, 43–70.

Smeck, N.E., Runge, E.C., Mackintosh, E.E., 1983. Dynamics and genetic modelling of soil systems. In: Wilding, L.P., Smeck, N.E., Hall, G.F. (Eds.), Pedogenesis and Soil Taxonomy, I. Concepts and Interactions. Elsevier, Amsterdam, pp. 51–81.

Soil Survey Staff, 1999. Soil taxonomy: a basic system of soil classification for making and interpreting soil surveys. USDA-SCS Agric. Handbook, vol. 436. U.S. Gov. Printing Office, Washington, DC.

Trombotto, D., 1998. Paleo-permafrost in Patagonia. Bamberger Geographische Schriften Band 15, 133–148.

Tyurin, I.V., 1951. Analytical procedure for a comparative study of soil humus. Trudy Pochvennogo Instituta Dokuchayeva 38, 5–9.

U.S. Salinity Laboratory Staff, 1954. Diagnosis and Improvement of Saline and Alkali Soils, Handbook, vol. 60. U.S. Department of Agriculture, Washington, DC.

Velde, V., 1985. Clays minerals: A physico-chemical explanation of their occurrence. Developments in Sedimentology, vol. 40. Elsevier, New York, p. 427.

Vogt, T., del Valle, H., 1994. Calcretes and cryogenic structures in the area of Puerto Madryn (Chubut, Patagonia, Argentina). Geografiska Annaler 76 A (1-2), 57–75.

Vogt, T., Larqué, P., 1998. Transformations and neoformations of clay in the cryogenic environment: examples from Transbaikalia (Siberia) and Patagonia (Argentina). European Journal of Soil Science 49, 367–376.

Watson, A., 1985. Structure, chemistry and origin of gypsum in southern Tunisia and in central Namib Desert. Sedimentology 32, 855–875.

Watts, N.L., 1978. Displacive calcite: evidence from recent and ancient calcretes. Geology 6, 699–703.

Watts, N.L., 1980. Quaternary pedogenic calcretes from the Kalahari (southern Africa): mineralogy, genesis and diagenesis. Sedimentology 27, 661–686.

Weaver, C.E., Beck, K.C., 1977. Miocene of the S.E. United State: a model for chemical sedimentation in a peri-marine environment. Sedimentary Geology 17, 1–234.

Williams, D.E., 1948. A rapid manometric method for the determination of carbonate in soils. Soil Science Society of America Proceedings 13, 127–129.

Wright, V.P., 1990. A micromorphological classification of fossil and recent calcic and petrocalcic microstructures. In: Douglas, L.A. (Ed.), Soil micromorphology: A basic and applied science. Developments in Soil Science, vol. 19. Elsevier, Amsterdam, pp. 401–407.

Wright, V.P., Tucker, M.E., 1991. Calcretes: an introduction. In: Wright, V.P., Tucker, M.E. (Eds.), Calcretes. International Association of Sedimentologists, Reprint Series, vol. 2. Blackwell, Oxford, pp. 1–22.

Yaalon, D.H., Wieder, M., 1976. Pedogenic palygorskite in some arid brown (Calciorthid) soils of Israel. Clay Minerals 11, 73–80.

Zelazny, L., Calhoun, F., 1977. Palygorskite (attapulgite), sepiolite, talc, pyrophylite, and zeolites. In: Dixon, J.B., Weed, S.B. (Eds.), Minerals in Soil Environments. Soil Science of America, Madison, WI, pp. 435–470.